J Mater Sci: Mater Med (2008) 19:3621–3629
DOI 10.1007/s10856-008-3477-3

Coagulation property of hyaluronic acid–collagen/chitosan complex film

Yangzhe Wu · Yi Hu · Jiye Cai · Shuyuan Ma · Xiaoping Wang

Received: 29 March 2008 / Accepted: 15 May 2008 / Published online: 19 July 2008

Abstract Biomacromolecule has been widely used as biomedical material. Because different biomacromolecules possess different properties, how to exhibit the respective advantages of different components on one type of biomaterial becomes the hot spot in the field of biomaterial studying. This work reported a type of complex film that consisted of hyaluronic acid (HA), type I collagen (Col-I), and chitosan (CS) (HA–Col-I/CS, HCC). Then, a series of experiments were performed, such as inverted microscopic observation, atomic force microscopic (AFM) imaging, flow cytometry (FCM) measurement, MTT assay, and MIC assay. In the present work, we observed the growing condition of 3T3 fibroblasts on the surface of the HCC complex film, visualized the morphological changes of platelets during the coagulation process, and discovered microparticles on the platelet membrane. Moreover, we confirmed the microparticles are the platelet-derived microparticles (PMPs) using the FCM. In addition, the minimal inhibitory concentration (MIC) of HCC against *Escherichia coli* (*E. coli*) 8099 was 0.025 mg/ml, against *Staphylococcus aureus* (*S. aureus*) ATCC 6538 was 0.1 mg/ml. The results together indicated that the HCC film possessed promising coagulation property, cell compatibility and anti-bacteria property, and the potential in future clinical application such as wound healing and bandage.

Yangzhe Wu and Yi Hu contributed equally to this work.

Y. Wu · Y. Hu · J. Cai (✉)
Department of Chemistry, Jinan University, Guangzhou 510632, People's Republic of China
e-mail: tjycai@jnu.edu.cn

S. Ma · X. Wang
The First Affiliated Hospital, Jinan University, Guangzhou 510632, People's Republic of China

1 Introduction

Biocompatible and biodegradable biomaterial such as hyaluronic acid (HA), type I collagen (Col-I), and chitosan (CS) have been widely used as biomedical engineering materials [1]. HA is a glycosaminoglycan with anti-inflammatory and anti-edematous properties, and it is the main component of cellular matrix (CM). HA interacts with proteins such as CD44, RHAMM, and fibrinogen, and plays an important role in many natural processes such as cell motility, cell adhesion, and wound healing [2, 3]. However, HA, as a biomaterial, possessed a disadvantage of easy degradation, therefore, to decrease the degradation rate, the modifications such as crosslinking with other biomolecules become imminent in application.

Collagen (including Col-I) is a glycoprotein and also a component of CM, and could promote wound healing [4]. Collagen is mainly used as coagulation material, and there are many reports about its clinical application. The coagulation mechanism of collagen mainly includes (a) coagulation factors activation, (b) inducing platelets adhering, activation, and accumulation, and (c) blocking the bleeding wound [5, 6]. As the ideal coagulation material, natural collagen possesses the optimal efficiency; however, collagen modification is necessary due to its low stability and weak mechanical strength [7] and fast degradation speed [8, 9].

CS is a kind of unique natural alkalescence polysaccharide molecule that consists of double helix structure. CS film is easily prepared due to its physicochemical

properties such as adhesion property, permeability, and tensile strength. In our previous work, the molecular chains and self-assembly structures of CS have been studied in detail [10]. Up to now, biocompatible CS film has been extensively applied as biomedical materials [11, 12] and there have many related reports, for example, used it as coagulation and anti-bacteria material. CS film possesses favorable hygroscopic property and air permeability due to its mesh structures [10]. However, CS itself is not an ideal coagulation material, and it is often blended with collagen, coagulation factors or $CaCl_2$ in application.

Platelets play a very important role in coagulation and could promote hemostasis and thrombosis. Morphological and functional changes of platelets could help us evaluate the properties of coagulation material. Membrane space configuration will change and the platelet-derived microparticles (PMPs) will be released in the activated platelets, then the exposed platelet glycoprotein IIb–IIIa receptor complex will interact with fibrinogen and result in platelet accumulation [13–16], and ultimately the chain reaction of coagulation will be initiated. Up to now, platelets were studied mainly based on flow cytometry (FCM) [17–21] and electron microscope (EM) however, there is rare high-resolution image data to locate where the PMPs released from platelet membrane. Atomic force microscope (AFM), a powerful tool of bio-imaging [22–24], has been extensively applied in biomaterial studying [25–27]; however, there are only a few AFM studies on platelets [28, 29].

To exert the advantages and avoid disadvantages, HA was firstly mixed with type I collagen (Col-I) and then assembled on the CS film. The properties of prepared HCC complex film (HA–Col-I/CS) were characterized by AFM, inverted microscope and FCM, and MTT assay and MIC assay were also performed. The results indicated that HCC complex film possessed promising cell compatibility, coagulation property and anti-bacteria efficiency, which determined the extensive applications of HCC complex film, such as curing the injured skin tissue, wound healing, and bandage. In addition, the convincing PMP images of this work provided complementary data for the studies of the process and mechanism of platelet activation and coagulation.

2 Materials and methods

2.1 Preparation of biomacromolecule film

2.1.1 Type I collagen film

The newly peeled mica was firstly treated with 0.1 M $NiCl_2$ solution to make mica electropositive, and then type I collagen (Col-I, 1 mg/ml, Sigma) solution was assembled on the surface of mica by electrostatic interaction, and air dried at room temperature.

2.1.2 HCC complex film

In our experiments, the concentration of CS (low molecular weight, Sigma) was 10 mg/ml, and that of HA (Sigma), Col-I (Sigma) were 2 mg/ml, respectively. CS polycation (dissolved in 2% acetic acid solution) was assembled on the surface of the newly peeled mica (without $NiCl_2$ treatment) and air dried at room temperature; and then the fully mixed and crosslinked solution of Col-I and HA (V:V = 1:1) was assembled on the surface of CS film (HA–Col-I/CS), and air dried at room temperature.

To determine the superiority of cell growth and proliferation of HCC complex film, we prepared six types of film (including HCC) in the six-well plates for the next step cell culture (the prepared film have similar structure to that prepared on mica). The procedure (including the concentration of samples) was similar to the preparation of HCC, and these films are also a two-layer system similar to the HCC-film. To improve the stability of films that prepared for cell culture, glutaraldehyde was used as crosslinker in some groups. After the pH value of the CS film was adjusted to 7.4 using 1 M NaOH and air-dried, glutaraldehyde was dropped on CS film and then washed with PBS, and then the other components of complex film were assembled on CS film. These prepared films were film 1, CS; film 2, Col-I/CS (without crosslinker: glutaraldehyde); film 3, Col-I/CS (containing crosslinker glutaraldehyde); film 4, HA–Col-I/CS (without crosslinker); film 5, HA–Col-I/CS (containing crosslinker); film 6, HA/CS (containing crosslinker). Furthermore, to further examine the superiority of HCC on promoting the cell proliferation, the MTT assay was performed: film 2 (designated as film b); film 4 (designated as film c); film 1 (designated as film d); film e, CS + HA.

2.2 Platelet isolation

Venous blood was drawn from healthy, aspirin free adult donors. The whole blood was drawn into 3.8% sodium citrate anti-coagulant (Sigma) in the volume ratio of 1:9. After centrifuging at the speed of 800 rpm for 10 min at 21°C, we pipette the upper 75% of the yellow supernatant fraction of platelet-rich plasma (PRP) from the polyethylene tube, and transfer it to another polyethylene tube, and the platelets were washed by centrifuging the PRP at 3,000 rpm for 10 min, then removed the supernatant and resuspended the platelets in PBS. The platelet washing procedure was repeated triple. After the whole washing process, the platelets were left resting for 20 min at room temperature (21°C) to allow them to return to their resting shape: discoid shape.

2.3 Platelet activation and membrane protein labeling

Platelet activation and membrane protein labeling were performed by the following processes. Briefly, five samples of 100 μl PRP were firstly added into five centrifugated tubes, and then HCC (10 μl), HA (10 μl), and CS (10 μl) solution were added into three tubes, respectively, and gently mixed them up together, then incubated in the dark at room temperature for 5 min, and the tubes for the control group and isotype IgG1 group were resting. Twenty microliter solution from each tube of the control and test groups was added into another five new tubes, respectively; 10 μl FITC-anti-CD41 and 10 μl PE-anti-CD62P were added into control group, 10 μl PE-anti-IgG1 was added into isotype group; 10 μl FITC-anti-CD41 and 10 μl PE-anti-CD62P were added into three test tubes, respectively (FITC-anti-CD41, PE-anti-CD62P, and PE-anti-IgG1 were from JingMei Co., China). Then gently mixed them up together and incubated in the dark at room temperature for 15–20 min. Then 500 μl paraformaldehyde was added into every tube and incubated at 2–8°C for 30 min. The prepared samples were analyzed by FCM (FACSCalibur, Becton Dickinson, USA) at 24 h.

2.4 3T3 fibroblast culture

The 3T3 fibroblast used in the study was provided by (Biopharmaceutical R&D Center of Jinan University, Guangzhou). Cells were cultured in RPMI 1640 medium with 20% fetal bovine serum (FBS) (Sijiqing Bio Co., China) in a humidified incubator under 5% CO_2. The cell proliferation curve of 3T3 fibroblasts that cultured on bio-complex film was measured with the cytometry.

2.5 MTT assay

Methylthiazolyl tetrazolium (MTT) assay could determine the level of cellular energy metabolism and indicate the condition of cell proliferation indirectly. The cellular concentration of 3T3 cells in logarithmic growth period was adjusted to 5×10^4 using culture medium (RPMI 1640) containing 10% FBS, then transferred the cellular solution into 96-well plate (100 μl every well), whose wells were covered by different types of complex films prepared beforehand, and then the cells cultured at 37°C (5% CO_2) for 24 h. Fifteen microliters of MTT (5 mg/ml, Sigma) was added into every well and incubated for 4 h, then culture medium was discarded; 150 μl DMSO was added into every well and incubated at room temperature for 40 min. The optical density (OD) was measured at 570 nm wavelength. Then the condition of cell proliferation could be determined according to the OD value.

2.6 MIC assay

Minimal inhibitory concentration (MIC) assay was performed at Guangdong Detection Center of Microbiology. *E. coli* 8099 and *S. aureus* ATCC 6538 in logarithmic growth period were diluted with 0.01 M PBS–10^6 CFU/ml. Fifty microliters of *E. coli* and *S. aureus* were mixed with 50 μl double diluted HCC solution (10 mg/ml CS, 2 mg/ml type I collagen, 2 mg/ml HA), respectively, and transferred them into 96-well plates and cultured at 37°C for 20 h. Then the OD value was measured at 600 nm wavelength.

2.7 AFM observation

The prepared samples were observed using AFM (CP-Research, Veeco, USA). Images were acquired at room temperature in the tapping mode in air. The curvature radius of the silicon tip is less than 10 nm and the force constant about 3 N/m, the length, width and thickness of tip cantilever are 215–235 μm, 30–40 μm, 3.5–4.5 μm, respectively, and the oscillation frequency of tip is 72–96 kHz (manufacturer offered). Scan rate is 0.6–1 Hz and the scanning range of scanner is 100 μm. The acquired images (256 × 256 pixels) were processed with the provided software (Image Processing 2.1, IP 2.1) to eliminate low-frequency background noise in scanning direction, and statistical analysis of data was based on the software IP 2.1, and presented as average ± SD. As for platelet observation, several microlitres of isolated platelet was dropped on the surface of the prepared film, then fixed using 2.5% glutaraldehyde (Sigma) for 10 min, and then washed three times using ultrapure water, air dried at room temperature in air for AFM observation.

2.7.1 3T3 cell observation

3T3 fibroblast cultured on the bio-complex film was fixed using 2.5% glutaraldehyde for 10 min and then observed directly.

3 Results and discussion

3.1 Characterization of cell compatibility of HCC complex film

To determine the superiority of cell growth and proliferation on HCC complex film, cellular growth condition on films was observed using Inverted Microscope (Leica, Germany) after cultured for 24 h, and cell were further visualized using AFM (Fig. 1).

The control group was shown in Figs. 1a and 3, T3 fibroblasts spread well and connected with each other, it is

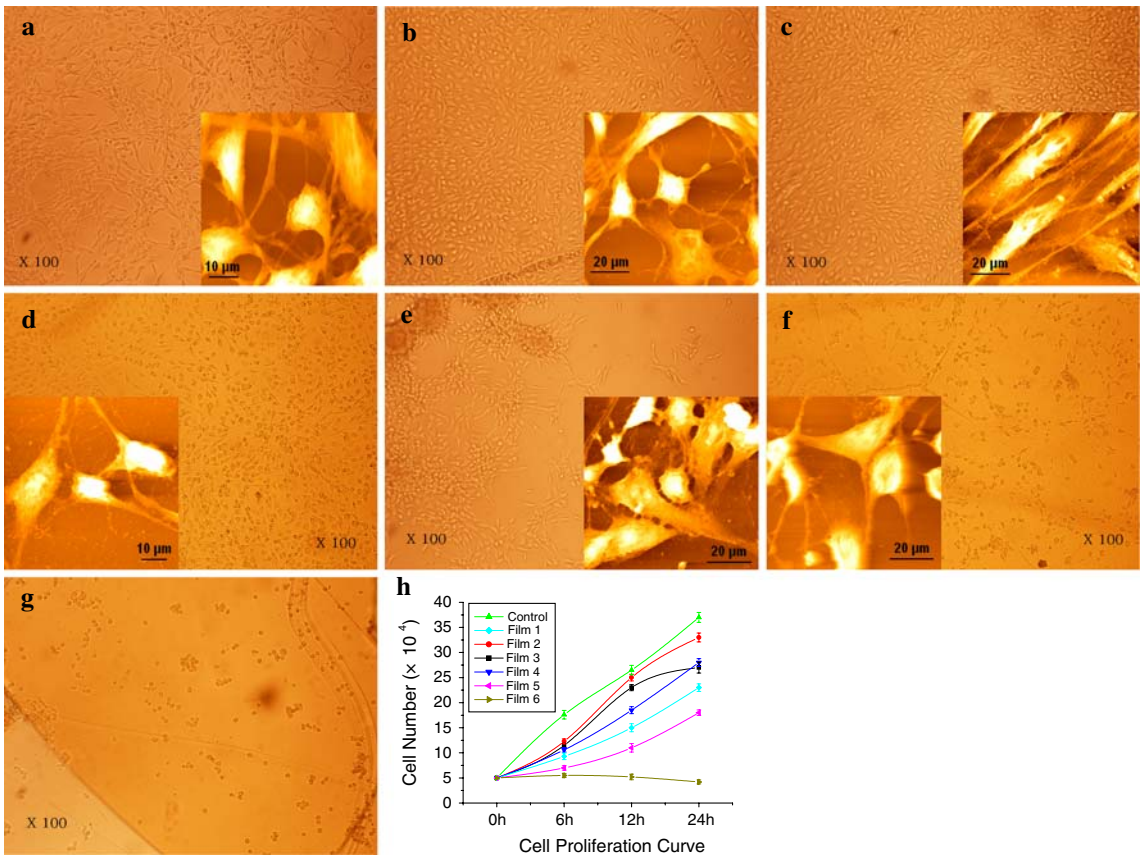

Fig. 1 The optical and AFM images of 3T3 fibroblasts. (**a**) Control group, (**b**–**g**) cells cultured on film 1 (CS), film 2 (Col-I + CS, without crosslinker: glutaraldehyde), film 3 (Col-I + CS, containting crosslinker), film 4 (HA + Col-I + CS, without crosslinker), film 5 (HA + Col-I + CS, containing crosslinker), and film 6 (HA + CS, containing crosslinker). The cellular growth condition of (**a**–**d**) was good, cells connected each other and even presented spindle-shaped (**c**); however, cells of (**e**) and (**f**) only grew locally. Cellular growth condition of (**g**) was bad and cells could not adhesive to the film surface. (**h**) Showed the cell proliferation curve on different film. Scanning range of AFM images were 60 μm (**a**), 90 μm (**b**), 90 μm (**c**), 70 μm (**d**), 80 μm (**e**), 80 μm (**f**), respectively

shown that cellular growth condition was good. Figure 1b showed cells cultured on CS film, cellular growth condition was good, whereas cells did not spread fully, which was due to the smooth surface and/or the single chemical composition of CS film. Figure 1c showed cells cultured on CS + Col-I film (without crosslinker), the results indicated that cellular growth condition was good, cells spread fully and presented spindle-shape, which meant that the CS + Col-I film could promote cell proliferation and growth of 3T3 fibroblasts. The difference between Fig. 1d (film 3) and c (film 2) was that in Fig. 1d, glutaraldehyde was added as a crosslinker to crosslink the CS and Col-I components. Figure 1e (film 4) showed cells cultured on HA + Col-I + CS (without crosslinker), and cells spread fully and presented spindle-shape, which elucidated the better growth conditions of cells, but cells only grew locally. This phenomenon could attribute to the fact that: HA, as a component of extra cellular matrix (ECM), could provide nutrition for cell growth, however, it is unsuitable for cell adhesion. Therefore, in our following MTT experiment, HA and Col-I were mixed fully and then assembled on the CS film to improve the cell compatibility of HCC complex film. Figure 1f (film 5) showed cells cultured on HA + Col-I + CS film containing glutaraldehyde, cellular growth condition was worse than that of Fig. 1e (film 4). Figure 1g (film 6) showed cells cultured on CS + HA film containing glutaraldehyde, the results indicated that cells could not adhere to the complex film at all, which supported the results of Fig. 1e (film 4) that HA is not suitable for cellular adherence, and these observed results were accordant with the result of cell proliferation curve (Fig. 1h). The results (Fig. 1c, e, h) seemed that the HCC film did not promote the cell proliferation effectively. This phenomenon could be ascribed to the fact that: HA, as a component of ECM, could provide nutrition for cell growth, however, it is unsuitable for cell adhesion. Therefore, in our following MTT experiment, HA and Col-I were mixed fully and then assembled on the CS film to improve the cell compatibility of HCC complex film. In addition, according to the results of cell growth, though the

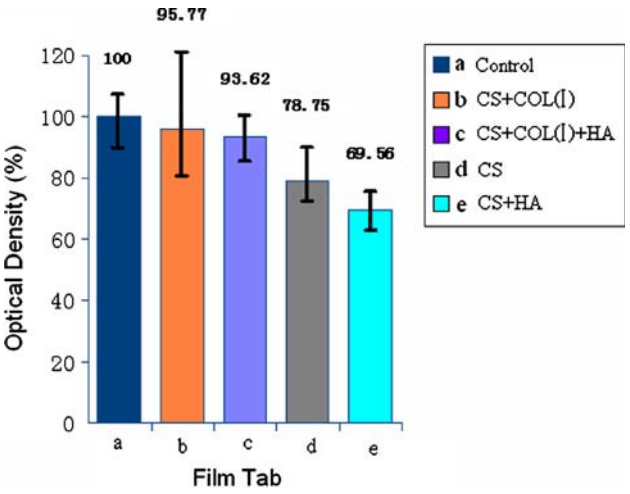

Fig. 2 The MTT assay result of 3T3 fibroblasts incubated on different films for 24 h. The OD value of the control group was set as 100% and the percentages of different films was figured out correspondingly, and vertical ordinate and horizontal ordinate represent percentage value of OD and the film notations, respectively ($n = 6$, $P < 0.05$)

crosslinker glutaraldehyde did not affect cell growth obviously, in the following experiment we did not use crosslinker because of the potential negative effects such as cytotoxicity.

To further determine the superiority of cell growth and proliferation on HCC complex film, a comparative analysis of MTT assay was performed, including four types of film (b–e) (see Sect. 2.1). Figure 2 showed the MTT assay results of 3T3 fibroblasts incubated on different films, which indicated that the OD value of cells cultured on film b and film c were higher than that of other groups. Though the OD value of film c is slightly lower than that of film b, however, biocompatible HA was still used as one component of the HCC complex film, because HA could be the nutrition in the process of cell growth and proliferation. Together, the results of microscopic observation and MTT assay indicated that the prepared HCC complex film possessed favorable cell compatibility due to the biocompatible components [30–33].

3.2 The evaluation of coagulation property of HCC complex film

3.2.1 AFM analysis of platelets on HCC complex film

The morphological changes of platelets and adsorptive capacity of platelets adhered to biomaterial surface were important parameters of coagulation property of biomaterial [34]. The process of fibrinogen secreted from the activated platelets induced by Col-I film had been studied [11] prior to the evaluation of coagulation property of HCC complex film, AFM observation indicated that the α particles and fibrinogen secreted from the activated platelets could result in platelets aggregation. Here, HA and Col-I were firstly mixed fully, and then assembled on the surface of CS film, therefore, the promising procoagulant property and anti-bacteria efficacy of the prepared HCC (HA–Col-I/CS) complex film could be expected.

Figure 3 showed the morphology of Col-I film (3a), HCC film (3b), and platelets (3c–f). The average roughness (Ra) of films is 1.401 nm (3a) and 8.838 nm (3b). Figure 3c showed a resting platelet with typical disk-like shape, whose diameter is 2.683 μm, height is 189.3 nm, and Ra is 84.74 nm. Moreover, the statistical results indicated that the size of resting platelets is 2.44 ± 0.51 μm in diameter and 112.37 ± 46.11 nm in height. Figure 3d–f showed platelets interacted with Col-I film. Macroscopic image (3d) indicated that platelets were in dispersing state, and there were no pseudopodium between platelets, however, microscopic image (3e) of single platelet indicated that platelets were in dendrite shape and pseudopodium were obvious (white arrows in 3e). Figure 3f was the enlarged view of the square frame in Fig. 3e, in which the cluster particles could be observed (black arrows), and the Ra of platelet surface was 72.14 ± 5.12 nm according to the statistical results of 25 platelets.

Large-scale images indicated that the great majority of platelets accumulated after interacted with HCC film. Microscopic images of AFM further visualized the spreading and accumulating behavior of platelets (Fig. 4). Figure 4a, d was the error signal mode images (some

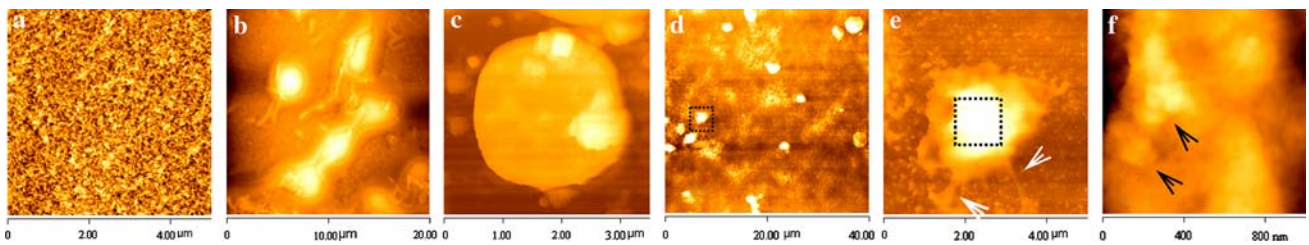

Fig. 3 Morphology of Col-I film (**a**), HCC film (**b**), and single resting platelet (**c**). The average roughness (Ra) of films is 1.401 nm (**a**) and 8.838 nm (**b**). (**d**) Platelets on the surface of Col-I film, (**e**) the enlarged view of the square frame in (**d**), (**f**) the enlarged view of the square frame in (**e**)

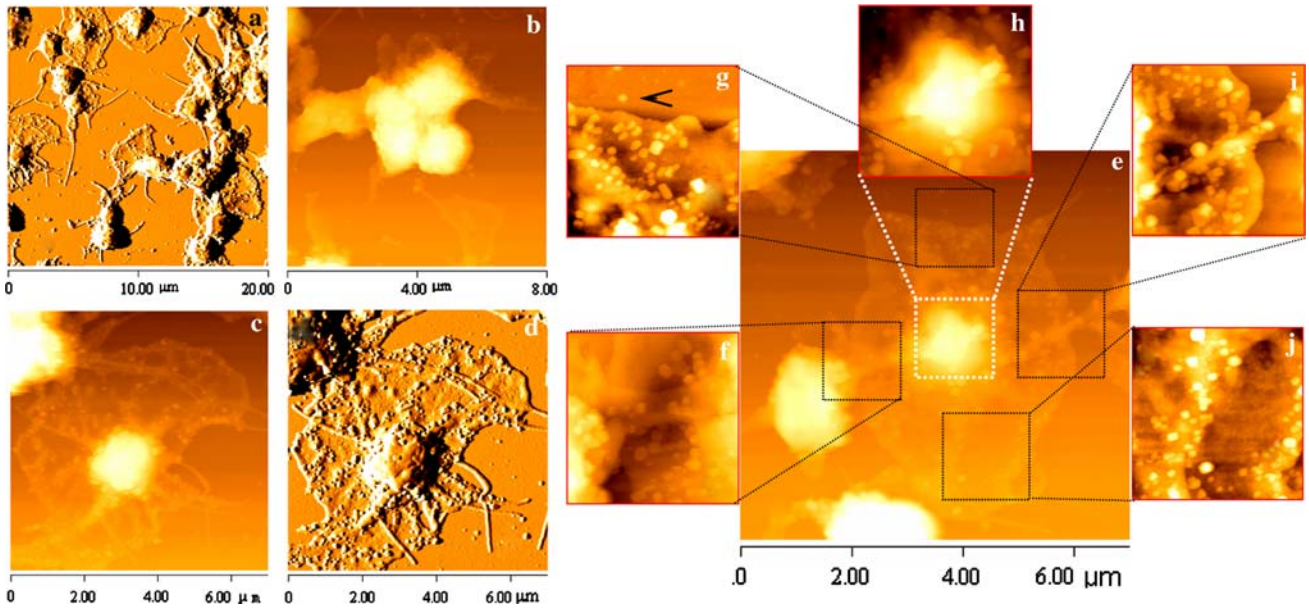

Fig. 4 AFM images of platelets on the HCC film. Dendritic, spreading and accumulated platelets (**a**–**e**) on the HCC film, there are a lot of microparticles (PMPs) on the whole body of the platelets; (**f**–**j**) enlarged views of the respective square frames in (**e**), and the scan range is 2 μm (**f**–**j**); (**a**, **d**) is the error signal mode image

details can be more easily distinguished in this image mode). The results of AFM imaging indicated that the great majority of platelets were in dendrite and spreading state (4c, e), in which the pseudopodium were obviously presented, and some platelets were in accumulation state (4a, b). It was more important that there were large numbers of microparticles on the surface of spreading platelets (4c–e), and the ultrastructural images (4f–j) of Fig. 4e more obviously visualized these microparticles with various sizes. AFM observation indicated that the particle density of the center was larger than that of the edge, which suggested that the microparticles were diffusing from the center to the edge. According to AFM analysis, these microparticles were PMPs, and our further data supported this view (see below). Moreover, the statistical results of PMPs size were showed as Fig. 5a, which indicated that PMPs size mainly distributed between 60 and 110 nm.

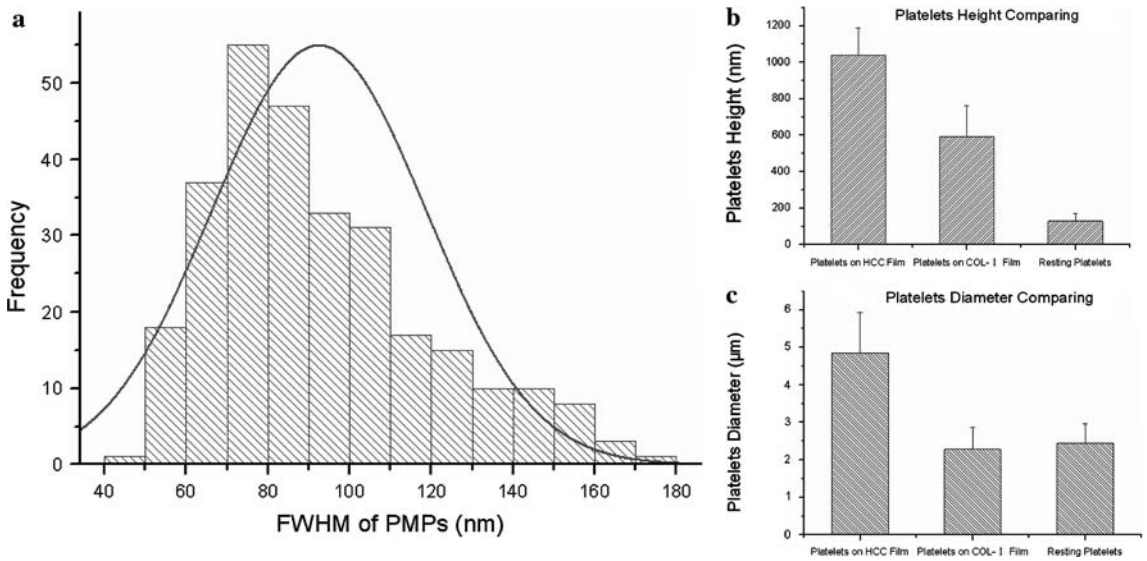

Fig. 5 (**a**) Statistical results of PMPs size (full wave at half maximum, FWHM). (**b**, **c**) The statistical height and diameter value of platelet after interacted with HCC film and Col-I film, respectively. The diameter and height of resting platelets were 2.44 ± 0.51 μm and 130.19 ± 39.33 nm, and that of platelets interacted with Col-Ifilm were 2.28 ± 0.58 μm and 592.62 ± 169.06, and after interacted with HCC film were 4.85 ± 1.08 μm and 1039.16 ± 148.43 nm, respectively

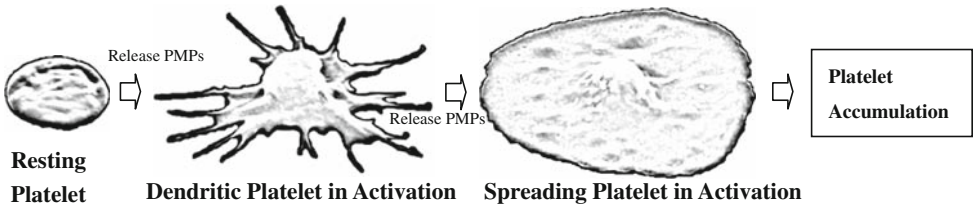

Fig. 6 The illustration map of activation process of the human platelet

To clarify the difference of platelets respectively interacted with Col-I film and HCC film, a comparative analysis was performed (Fig. 5b, c), which indicated that HCC film could activate platelets more effectively than pure collagen film. This result might relate to the larger Ra of HCC film (Fig. 3) and more suitable for platelets adherence, which induced the larger contact area between HCC film and platelets. Moreover, the different chemical composition at the interface might also influence the platelet activation. To our knowledge, according to the changes of diameter, height, and morphology, the activated state of platelets could be divided into five stages: rotundity, dendrite shape, transition, spreading, and accumulation. The majority of platelets on Col-I film were in the activation stage of dendrite shape (Fig. 3e), and there were no PMPs on the surface of platelets. However, on the HCC film, the majority of platelets were at transition and spreading stage and some were at the stage of accumulation, and there were large numbers of PMPs on the surface of platelets (60–110 nm), and meanwhile, a few PMPs were also observed on material surface (black arrow in Fig. 4g). Figure 6 illustrated the activation process of the human platelet. In addition, the Ra of platelet surface (on HCC film) was 215.20 ± 22.74 nm according to the statistical results of random 25 platelets.

Together, according to the results of AFM visualization, HCC film possessed promising coagulation property. Moreover, HCC film possessed the locus for platelets adherence and could induce the release of platelet α granule to form microparticles (PMPs) on the platelet surface. On the other hand, previous studies [35] indicated that PMPs were the result of the budding of pseudopodium, and the PMPs formation was closely related to unique morphological changes in activated platelets, especially pseudopod formation, which might be the results of intracellular cytoskeletal reorganization. However, our AFM images indicated that PMPs were released not only from near the tip of pseudopodium [35], but also from the whole platelet surface, which narrated that PMPs were the result of the budding of the whole platelet body.

3.2.2 *Flow cytometry (FCM) analysis of platelet membrane protein*

Activated platelets could release PMPs, which possess integrated membrane structure and express platelet membrane glycoprotein such as GPIIb/IIIa complex and P selectin. The released PMP is the indicator of the activated platelet.

To testify the released microparticles of activated platelets in Fig. 4 were the PMPs, we examined the expression of platelet surface glycoprotein CD 41 and CD 62P (P selectin). Both resting and activated platelets would express GP CD41, however, only the activated platelets would express CD62p, which could be the specific and sensitive marker of activated platelets.

The results of FCM indicated that expression of FITC-anti-CD41 in resting platelets (blank control group) was 99.46%, however, resting platelets did not express PE-anti-CD62P. Then, an isotype control analysis (PE-anti-mouse IgG1) was performed to exclude the background interferences of non-specific recognition, such as T and B cells, and the results in Fig. 7 indicated that there were no non-specific interferences because of the negative expression of PE-anti-mouse IgG1.

As for test groups (Fig. 8), we performed three testing groups that included HCC (tube 1), CS (tube 2), and HA (tube 3). Tube 1, after platelets interacted with 0.1 mg/ml HCC solution, the expression of FITC-anti-CD41 was 87.70% and that of PE-anti-CD62P was 12.09%, which suggested that activated platelets released α granule that occupied the protein locus of CD41 and resulted in expression decreasing of CD41. After platelets interacted with 2 mg/ml CS (tube 2), the expression of FITC-anti-CD41 was 99.33% and that of PE-anti-CD62P was 0.46%,

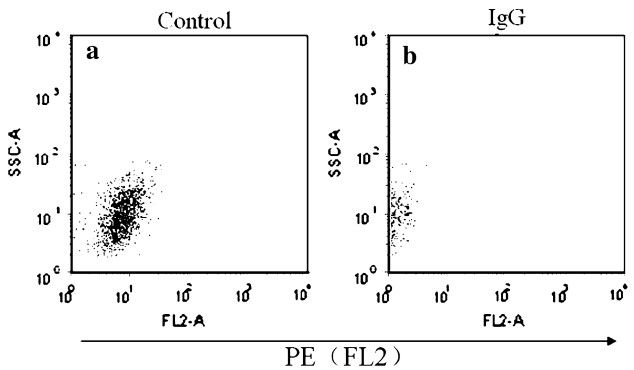

Fig. 7 The representative dot plots result. (**a**) The control group, FL2 represented the fluorescence intensity of mouse anti-human CD62P/PE; (**b**) The isotype control group, FL2 represented the fluorescence intensity of mouse IgG1 isotype control/PE. ($n = 3$, $P < 0.05$)

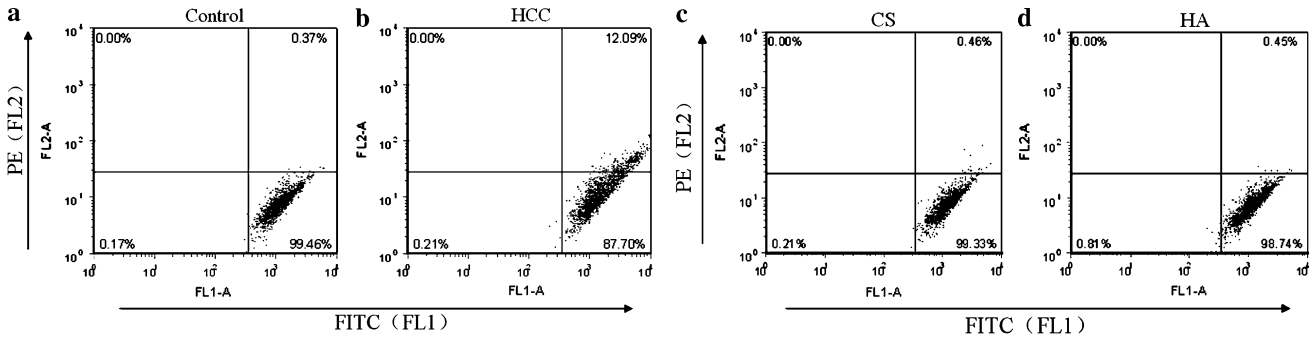

Fig. 8 The representative FITC/PI double staining dot plots result. (**a**) The control group, in which platelets were in their resting stage, showed that the platelet rich plasma (PRP) could express mouse anti-human CD41/FITC by 99.46%, while there was no expression of anti-human CD62P(P-selectin)/PE (0.37%); (**b**) the experimental group showed that when the PRP was interacted with the HCC fluid, the percentage of platelets that could express mouse anti-human CD41/FITC is 87.70%, while the expression of anti-human CD62P(P-selectin)/PE increased to 12.09%; (**c**, **d**) when the PRP was interacted with two main components of the HCC complex film: CS and HA solution, respectively, the expression ratios of mouse anti-human CD41/FITC and anti-human CD62P(P-selectin)/PE showed no significant difference compared with the control group by statistic evaluation ($n = 3$, $P < 0.05$)

which indicated that CS could not activate platelets. As for HA (tube 3), the expression of FITC-anti-CD41 was 98.74% and that of PE-anti-CD62P was 0.46%, which indicated that HA could not activate platelets by itself too. Because type I collagen is a natural coagulant, and CS and HA cannot induce platelet activation, these results altogether confirmed that Col-I component of HCC complex film played a key role in procoagulant process. Furthermore, the results of FCM also supported the results of AFM observation (Figs. 3 and 4), HCC complex film could effectively induce platelets to release PMPs, and on the other hand, the microparticles that AFM observed on the surface of activated platelets (Fig. 4) were PMPs.

A series of variation such as morphological changes, pseudopodium formation, PMPs release and CD62P exposure were closely related to platelet activation, and the PMPs were the result of the release of inner α granule in activated platelets. Up to now, PMPs assay were mainly based on FCM [20, 36–39], however, the direct image data were not enough. Siedlecki et al. [40] only observed the PMPs on the material surface; Cauwenberghs et al. [41] observed the PMPs on the surface of fibrinogen substrate and at the tip of platelet pseudopodium, however, there is rare image data to locate where the PMPs released from platelet membrane. Yano's study [35] indicated that the size of most of the PMPs was less than 0.5 μm, our AFM results further quantified the size of the PMPs, 60–110 nm. Thanks to the high resolution of AFM images, we determined the release location and the size range of PMP particles on the platelet membrane.

3.3 The evaluation of anti-bacteria property of HCC complex film

To provide experimental data for future application, we further evaluated the anti-bacteria property of HCC complex film. Previous studies had proved the promising anti-bacteria efficiency of CS [42–44]. The assay results indicated that HCC complex film possessed favorable anti-bacteria property, the MIC of HCC against *E. coli* 8099 was 0.025 mg/ml, against *S. aureus* ATCC 6538 was 0.1 mg/ml.

4 Conclusion

In the present study, a type of multi-function biomacromolecule complex film, whose components included HA, Col-I, and CS (HA–Col-I/CS, HCC) and could be used to promote wound healing, was prepared. The experimental results indicated that HCC complex film possessed promising coagulation capability, cell compatibility and anti-bacteria property. Moreover, the PMPs in activated platelets were visualized and analyzed in detail based on AFM and FCM, the PMPs size was 60–110 nm. Our results provided the necessary and valuable data for the next experiments and future application of HCC film as a type of procoagulant material.

Acknowledgments We thank associate professor Meiying Zhang (Biomedicine Research & Development Center, Jinan University) for her warm help in cell culture techniques. This work is supported by the NSFC (No. 60578025, 30540420311).

References

1. Q. Feng, G. Zeng, P. Yang et al., Colloid Surf. A **257–258**, 85 (2005)
2. T. Yamada, T. Kawasaki, J. Biosci. Bioeng. **99**, 521 (2005)
3. K.M. Stuhlmeier, Wien. Med. Wochenschr. **156**, 563 (2006)
4. W. Choi, H. Kawanabe, Y. Sawa et al., Acta Odontol. Scand. **66**, 31 (2008)
5. L.J. Alberio, K.J. Clemetson, Curr. Hematol. Rep. **3**, 338 (2004)
6. S. Ilveskero, P. Siljander, R. Lassila, Arterioscler. Thromb. Vasc. Biol. **21**, 628 (2001)

7. B.P. Chan, K.F. So, J. Biomed. Mater. Res. A **75**, 689 (2005)
8. L. Ma, C. Gao, Z. Mao et al., Biomaterials **25**, 2997 (2004)
9. L. Meinel, V. Karageorgiou, S. Hofmann et al., J. Biomed. Mater. Res. A **71**, 25 (2004)
10. Y. Hu, Y.Z. Wu, J.Y. Cai et al., Int. J. Mol. Sci. **8**, 1 (2007)
11. J.M. Dang, D.D. Sun, Y. Shin-Ya et al., Biomaterials **27**, 406 (2006)
12. T. Haque, H. Chen, W. Ouyang et al., Int. J. Artif. Organs **28**, 631 (2005)
13. G.J. Toes, D.J. van, J. Haan et al., Biomaterials **20**, 1951 (1999)
14. J. Wang, J.Y. Chen, P. Yang et al., Nucl. Instrum. Meth. B **242**, 12 (2006)
15. S.N. Rodrigues, I.C. Goncalves, M.C. Martins et al., Biomaterials **27**, 5357 (2006)
16. P. Fungaloi, E.R. Statius, Y.P. Wu et al., Photochem. Photobiol. **75**, 412 (2002)
17. C.X. Qu, J.Z. Wang, W.H. Wan et al., J. Clin. Lab. Anal. **20**, 250 (2006)
18. J.E. Fernandez-Barbero, P. Galindo-Moreno, G. Avila-Ortiz et al., Clin. Oral. Implants Res. **17**, 687 (2006)
19. M.D. Linden, A.L. Frelinger, M.R. Barnard et al., Semin. Thromb. Hemost. **30**, 501 (2004)
20. C. Aurigemma, A. Fattorossi, A. Sestito et al., Thromb. Res. **120**, 901 (2007)
21. L. Catani, M.E. Fagioli, P.L. Tazzari et al., Exp. Hematol. **134**, 879 (2006)
22. G. Binnig, C.F. Quate, C. Gerber, Phys. Rev. Lett. **56**, 930 (1986)
23. J.K. Horber, M.J. Miles, Science **302**, 1002 (2003)
24. J.L. Alonso, W.H. Goldmann, Life Sci. **72**, 2553 (2003)
25. S. Rammelt, T. Illert, S. Bierbaum et al., Biomaterials **27**, 5561 (2006)
26. C.A. Siedlecki, R.E. Marchant, Biomaterials **19**, 441 (1998)
27. M.D. Garrison, B.D. Ratner, Ann. N. Y. Acad. Sci. **831**, 101 (1997)
28. A. Blinca, J. Magdica, J. Fricb et al., Fibrinolysis Proteolysis **14**, 288 (2000)
29. I. Kang, M. Raghavachari, C.M. Hofmann et al., Thromb. Res. **119**, 731 (2007)
30. G. Abatangelo, R. Barbucci, P. Brun et al., Biomaterials **18**, 1411 (1997)
31. C. Jiansu, L. Qinhua, X. Jintang et al., Artifi. Organs **29**, 104 (2005)
32. J.S. Mao, H.F. Liu, Y.J. Yin et al., Biomaterials **24**, 1621 (2003)
33. T. Tanabe, N. Okitsu, A. Tachibana et al., Biomaterials **23**, 817 (2002)
34. M. Kanno, H. Kawakami, S. Nagaoka et al., J. Biomed. Mater. Res. **60**, 53 (2002)
35. Y. Yano, J. Kambayashi, E. Shiba et al., Biochem. J. **299**(Pt 1), 303 (1994)
36. A. Vidovic, M. Vilibic, A. Markotic et al., Psychiatry Res. **150**, 211 (2007)
37. T. Kalsch, E. Elmas, X.D. Nguyen et al., Thromb. Res. **120**, 703 (2007)
38. V. Serebruany, A. Malinin, A. Pokov et al., Thromb. Res. **119**, 175 (2007)
39. T. Kalsch, X.D. Nguyen, E. Elmas et al., Int. J. Cardiol. **111**, 217 (2006)
40. C.A. Siedlecki, I.W. Wang, J.M. Higashi et al., Biomaterials **20**, 1521 (1999)
41. S. Cauwenberghs, M.A. Feijge, A.G. Harper et al., FEBS Lett. **580**, 5313 (2006)
42. B. Li, J.F. Kennedy, J.L. Penga et al., Carbohydr. Polym. **65**, 488 (2006)
43. X. Wang, Y. Du, J. Yang et al., J. Biomed. Mater. Res. A **84**, 384 (2008)
44. L. Nan, C. XiGuang, P. HyunJin et al., Carbohydr. Polym. **64**, 60 (2006)